Correlation of the Product E/Z Framework Geometry and O/O vs O/N Regioselectivity in the Dialkylation of Hyponitrite

Navamoney Arulsamy, D. Scott Bohle,* Jerome A. Imonigie, and Elizabeth S. Sagan

Contribution from the Department of Chemistry, University of Wyoming, Laramie, Wyoming 82071-3838

Received December 3, 1999

Abstract: The products from the alkylation of silver hyponitrite with *tert*-butyl bromide, *tert*-amyl bromide, *p-tert*-butyl benzylbromide, and chlorotriethylsilane have been determined. In the reaction of *tert*-butyl bromide the formation of three new products, namely, (*Z*)-*N*-*tert*-butyl-*N*′-*tert*-butoxydiazene-*N*-oxide {$(CH_3)_3CN(O)NOC(CH_3)_3$}, **1D**, *trans*-mono-*O*-*tert*-butylhyponitrous acid {$(CH_3)_3CONNOH$}, **2A**, and (*Z*)-*N*-*tert*-butyl-*N*′-hydroxydiazene-*N*-oxide {$(CH_3)_3CN(O)NNOH$}, **2D**, is observed together with the formation of the known *trans*-di-*O*-*tert*-butyl hyponitrite {$(CH_3)_3CONNOC(CH_3)_3$}, **1A**. The reaction with *tert*-amyl bromide also yielded the corresponding *tert*-amyl derivatives. However, from the reactions of *p-tert*-butylbenzyl bromide and chlorotriethylsilane with silver hyponitrite, the corresponding *trans*-di-*O*-*tert*-alkylhyponitrites were obtained as the only alkylated products. The differential reactivity of the two sets of halides with silver hyponitrite is explained in terms of the higher stability of the cations generated from the former halides in comparison to those generated from the latter halides. The thermal decomposition data and UV−visible spectroscopic data are reported for all of the products. Crystallographic structural data are reported for two of the products, namely, (*Z*)-*N*-*tert*-butyl-*N*′-*tert*-butoxydiazene-*N*-oxide, **1D**, as its hyponitrous acid adduct, $(CH_3)_3CN(O)NOC(CH_3)_3 \cdot {}^1/_2HONNOH$, and *trans*-di-*O*-*p*-*tert*-butylbenzyl hyponitrite, $\{p(CH_3)_3C\}C_6H_4CH_2ONNOCH_2C_6H_4$-*p*-$\{C(CH_3)_3\}$. Theoretical calculations using ab initio density functional theory (B3LYP) are reported for the hyponitrite dianion, *trans*-mono-*O*-methylhyponitrite anion, (*Z*)-*N*-methyl-*N*′-hydroxylatodiazene-*N*-oxide anion, and for the methylation transition states. On the basis of the products isolated from the reactions of *tert*-butyl bromide and *tert*-amyl bromide and the theoretical calculations, a pathway is proposed to account for the observed product distributions where O/O-dialkylation is found in the *trans(E)* products and O/N-dialkylation is found in the *cis*(*Z*) products.

Several oxyanions of nitrogen are ambidentate nucleophiles which undergo either N- or O-alkylation reactions depending upon the incipient electrophile and the reaction conditions. Although this reactivity pattern is well-established for hydroxylamine[1,2] and nitrite,[3−5] it has not been well-demonstrated for the hyponitrite, peroxynitrite, or other oxy-anions of nitrogen. In the case of hyponitrite, there is only one report where the ambident nucleophilic nature of silver hyponitrite toward organic halide has been observed.[6] Bis-O-alkylation of hyponitrite is a well-known reaction, and the resulting *trans*-dialkylesters are commonly employed as polymerization initiators.[7−11]

The most widely employed synthetic route to the alkyl esters of hyponitrous acid involves the reaction of the appropriate alkyl halides with silver hyponitrite.[8,12−17] It has long been known that the reaction of *tert*-butyl- and *tert*-amyl halides with silver hyponitrite produces *trans*-di-*O*-*tert*-butyl[15,17] and *trans*-di-*O*-*tert*-amyl hyponitrites,[16,18] respectively. However, in principle, the reactions could produce no less than six isomers as shown in Figure 1, if hyponitrite's ambidentate nucleophilic behavior is coupled to facile E/Z isomerization.

The low yields that are commonly observed for the reactions of alkyl halides with silver hyponitrite have been attributed to possible competing elimination reactions and/or side reactions, whereas the possibility of the formation of other isomers is not addressed in detail.[6,18] Recently, we reported the synthesis and characterization of alkylammonium and base-stabilized hyponitrous acid salts which are stable at ambient temperature and soluble in a variety of organic solvents.[19] As part of our research into the oxy-anions of nitrogen, we were interested in the chemical reactivity of the hyponitrite anion. As will be described below, we have isolated *trans*-di-*O*-*tert*-butyl hyponitrite (**1A**), (*Z*)-*N*-*tert*-butyl-*N*′-*tert*-butoxydiazene-*N*-oxide (**1D**),[20] *trans*-mono-*O*-*tert*-butyl-hyponitrous acid (**2A**), and (*Z*)-*N*-*tert*-butyl-

(1) Harger, M. J. P. *J. Chem. Soc., Perkin Trans. 1* **1981**, 3284−3288.
(2) Harger, M. J. P. *J. Chem. Soc., Perkin Trans. 1* **1983**, 2699−2704.
(3) Kornblum, N.; Fishbein, L.; Smiley, R. A. *J. Am. Chem. Soc.* **1955**, *77*, 6261−6266.
(4) Kornblum, N.; Smiley, R. A.; Blackwood, R. K.; Iffland, D. C. *J. Am. Chem. Soc.* **1955**, *77*, 6269−6280.
(5) Kornblum, N. The Synthesis of Aliphatic and Alicyclic Nitro Compounds. *Org. React.* **1962**, *12*, 101−156.
(6) Quinga, E. M. Y.; Bieker, T.; Dziobak, M. P.; Mendenhall, G. D. *J. Org. Chem.* **1989**, *54*, 2769−2771.
(7) Zorn, W. *Ber. Dtsch. Chem. Ges.* **1878**, *11*, 1630−34.
(8) Hughes, M. N. *Q. Rev. Chem. Soc.* **1968**, *22*, 1−13.
(9) Ray, N. H. *J. Chem. Soc.* **1960**, 4023−8.
(10) Harris, I.; Marshall, I.; Jarrett, K. B. *Nature [London]* **1947**, *159*, 843.
(11) Dulog, L.; Klein, P. *Chem. Ber.* **1971**, *104*, 895−901.
(12) Hantzch, A.; Kaufmann, L. *Justus Liebigs Ann. Chem.* **1896**, *292*, 317−340.
(13) Partington, J. R.; Shah, C. C. *J. Chem. Soc.* **1932**, 2589−2597.
(14) Ho, S. K.; de Sousa, J. B. *J. Chem. Soc.* **1961**, 1788−1797.
(15) Kiefer, H.; Traylor, T. G. *Tetrahedron Lett.* **1966**, 6163−8.
(16) Walling, C.; McGuinness, J. A. *J. Am. Chem. Soc.* **1969**, *91*, 2053−2058.
(17) Ogle, C. A.; VanderKooi, K. A.; Mendenhall, G. D.; Lorprayoon, V.; Cornilsen, B. C. *J. Am. Chem. Soc.* **1982**, *104*, 5114−5119.
(18) Ogle, C. A.; Martin, S. W.; Dziobak, M. P.; Urban, M. W.; Mendenhall, G. D. *J. Org. Chem.* **1983**, *48*, 3728−3733.
(19) Arulsamy, N.; Bohle, D. S.; Imonigie, J. A.; Sagan, E. S. *Inorg. Chem.* **1999**, *38*, 2716−2725.

10.1021/ja994261o CCC: $19.00
Published on Web 05/24/2000

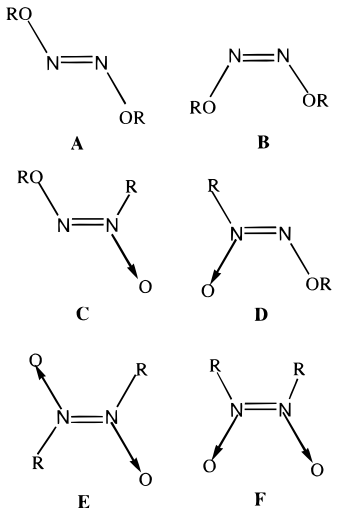

Figure 1. Six possible isomers for alkylation of $Ag_2N_2O_2$ with alkyl halides.

N′-hydroxydiazene-*N*-oxide (**2D**) from the reaction of *tert*-butyl bromide with silver hyponitrite by the slightly modified procedure of Kiefer et al.[15] Although a number of (*Z*)-*N*-alkyl-*N*-alkoxydiazene-*N*-oxides, RN(O)NOR with different organic groups[21−28] have been synthesized by other methods, there is only one instance in which an *N*-alkyl-*N*-alkoxydiazene-*N*-oxide has been isolated from the alkylation of silver hyponitrite.[6] In addition, there is no literature data on mono-alkyl hyponitrites resulting from the reaction of alkyl halides with silver hyponitrite. In view of these results, and given the current interest in this class of compounds, we decided to investigate the reactions of *tert*-butyl-, *tert*-amyl-, *p-tert*-butylbenzyl bromides, and chloro triethylsilane with silver hyponitrite more thoroughly to see if they exhibit ambident alkylation reactivity similar to nitrite. While the reactions of *tert*-butyl-[15] and *tert*-amyl[16,18] halides with silver hyponitrite have been reported to yield the corresponding *trans*-di-*O*-alkyl esters, those of *p-tert*-butylbenzyl bromide and chlorotriethylsilane with silver hyponitrite were heretofore unreported.

In this paper, we report (i) the synthesis, isolation, and characterization of four isomers of *tert*-butyl and *tert*-amyl hyponitrites; (ii) the synthesis and structural characterization of *p-tert*-butylbenzyl hyponitrite, *trans*-bis-*O*-triethylsilyl hyponitrite, and thallium hyponitrite; (iii) the thermal decomposition (DSC) and UV−vis spectroscopic studies of these compounds, and (iv) ab initio calculations for the ground states and vibrational frequencies for the dimethyl and methyl homologues for these compounds, and transition states for the O/N methylation of MeONNO$^-$. Taken together, these results demonstrate and lay the framework for understanding the ambiphilic character of hyponitrite alkylation.

Experimental Section

Materials and Methods. All chemicals and solvents were of reagent grade. The solvents were purified by standard techniques.[29] All of the organic halides were used without further purification except *tert*-butyl bromide, which was dried over molecular sieves and K_2CO_3 for 24 h and distilled. Sodium and silver hyponitrites were prepared by literature methods.[19] Silver hyponitrite was thoroughly dried at room temperature in a vacuum oven. IR spectra were recorded on a MIDAC FTIR instrument as potassium bromide pellets or as neat samples between KBr plates. Raman spectra were recorded on a Detection Limit Inc., Solution 633 Raman Laser System. UV−vis data were measured in methanol solvent at room temperature on a Hewlett-Packard 8452 diode-array spectrometer with quartz cuvettes. ^{1}H and ^{13}C NMR spectra were recorded on a Bruker 400 MHz instrument at room temperature using $CDCl_3$ with TMS (0.05% v/v) as internal reference. Elemental analyses were performed by either Atlantic Microlab, Norcross, GA or Galbraith Laboratories, Inc., Knoxville, TN.

Synthesis of $(CH_3)_3CN(O)NOC(CH_3)_3\cdot{}^1/_2$HONNOH {1D·$^1/_2$HONNOH}. This compound was prepared according to Kiefer and Traylor's[15] method except that the filtrate was evaporated at high vacuum to give X-ray quality crystals of *N*′-*tert*-butoxy-*N*-*tert*-butyl-*N*-diazene-oxide with a solvated hyponitrous acid molecule. The volatile products including the major product, *trans*-di-*O*-*tert*-butyl hyponitrite, were collected in the liquid nitrogen trap and left behind colorless crystals of **1D**·$^1/_2$HONNOH in the flask. Anal. Calcd for $C_{16}H_{38}N_6O_6$: C, 46.81; H, 9.33; N, 20.47%. Found: C, 46.74; H, 9.27; N, 20.75%. IR (KBr): 3207 b, 3061 m, 2987 m, 2947 w, 2826 w, 1485 s, 1397 m, 1375s, 1274 s, 1252 s, 11185 s, 1067 s, 1020 sh, 1004 vs, 991 vs, 929 sh, 844 s, 809 w, 693 b, 615 w, 571 m, 492 w, 467 m, 448 m cm^{-1}. ^{1}H NMR ($CDCl_3$) δ 9.55 (s, 1H, *H*ON), 1.57 (s, 9H, (C*H*$_3$)$_3$−C−N), 1.41 (s, 9H, (C*H*$_3$)$_3$−C−O); ^{13}C NMR ($CDCl_3$) δ 82.5, 73.5, 27.56, 27.49.The free ester, **1D**, was obtained as a colorless oil by passing the methylene chloride solution of the hyponitrous acid adduct through either a neutral preparative TLC plate or neutral alumina column using methylene chloride as eluent. Anal. Calcd for $C_8H_{18}N_2O_2$: C, 55.14; H, 10.41; N, 16.08%. Found: C, 55.17; H, 10.50; N, 16.01%. IR (neat): 2992 vs, 2938 s, 2880 sh, 1485 s, 1414 sh, 1391 m, 1368 vs, 1271 s, 1248 sh, 1184 s, 1061 s, 1038 sh, 1013 sh, 991 vs, 924 sh, 901 w, 849 vs, 808 w, 743 m, 571 vs, 554 sh, 488 m, 474 sh, 442 m, 424 w cm^{-1}. UV−vis (MeOH, λ_{max}, nm (ϵ)): 234 (7200 ± 80) M^{-1} cm^{-1}. ^{1}H NMR ($CDCl_3$) δ 1.56 (s, 9H, (C*H*$_3$)$_3$−C−N), 1.41 (s, 9H, (C*H*$_3$)$_3$−C−O); ^{13}C NMR ($CDCl_3$) δ 82.3, 73.6, 27.79, 27.75. Yields obtained from the above syntheses and from those described below are listed in Table 4.

Synthesis of *trans*-Di-*O*-*tert*-butyl Hyponitrite (1A) *trans*-Mono-*O*-*tert*-Butyl Hyponitrite (2A) and (*Z*)-*N*-*tert*-Butyl-*N*′-hydroxydiazene-*N*-oxide (2D). The crude product mixture was obtained from the reaction of silver hyponitrite and *tert*-butyl bromide in diethyl ether solvent as described by Kiefer and Traylor[15] except that the solvent was evaporated under a steady flow of nitrogen gas at room temperature. The isomers were separated either by column chromatography or on preparative silica gel TLC plate. First elution with hexane yielded exclusively the *trans*-di-*O*-*tert*-butyl hyponitrite, **1A**. The IR and NMR spectral features of the product are consistent with those reported in the literature.[15,17,30] Subsequent elution with methylene chloride separated the remaining products into three fractions. The first fraction contained *trans*-mono-*O*-*tert*-butyl hyponitrite (**2A**), the second fraction contained (*Z*)-*N*-*tert*-butyl-*N*′-*tert*-butoxydiazene-*N*-oxide (**1D**), and the third fraction contained a mixture of (*Z*)-*N*-*tert*-butyl-*N*′-hydroxydiazene-*N*-oxide (**2D**) and *tert*-butyl alcohol. *Note:* When preparative basic alumina TLC plate was used, **2A** decomposed completely to *tert*-butyl alcohol.

(20) In this manuscript the commonly used *trans*(*E*) and *cis*(*Z*) terms will be used to describe the stereochemistry of hyponitrite and its esters but for the alkylated diazenium diolates, which result from N-alkylation, the stereochemistry will be solely denoted as Z or E around N═N.

(21) Freeman, J. P. *J. Org. Chem.* **1963**, *28*, 2508−2511.
(22) Freeman, J. P.; Lillwitz, L. D. *J. Org. Chem.* **1970**, *35*, 3107−3110.
(23) Cherepinskii-Malov, V. D.; Marchenko, G. A.; Makhametzyanov; Buzykin, B. I. *Bull. Acad. Sci. USSR, Div. Chem. Sci.* **1985**, *34*, 871.
(24) Marchenko, G. A.; Chertanova, L. F.; Antipin, M. Y.; Struchkov, Y. T.; Punegova, L. N. *Dokl. Phys. Chem. (Engl. Transl.)* **1987**, *294*, 583−586.
(25) Atovmyan, L. O.; Golovinam, N. I.; Zyuzin, I. N. *Bull. Acad. Sci. USSR, Div. Chem. Sci.* **1987**, *36*, 1205−1208.
(26) Bohle, D. S.; Imonigie, J. A. *J. Org. Chem.* Manuscript submitted.
(27) George, M. V.; Kierstead, R. W.; Wright, G. F. *Can. J. Chem.* **1959**, *37*, 679−699.
(28) Hickmann, E.; Hadicke, E.; Reuter, W. *Tetrahedron Lett.* **1979**, 2457−2460.
(29) Perrin, D. D.; Armargo, W. L. *Purification of Laboratory Chemicals*, 3rd ed.; Pergamon Press: Oxford, U.K., 1988.
(30) Chen, H.-T. E.; Mendenhall, G. D. *J. Am. Chem. Soc.* **1984**, *106*, 6375−6378.

$(CH_3)_3CONNOH$ (2A). This compound is unstable at ambient temperature, and was spectroscopically characterized. IR (neat): 3418 b, 2986 s, 2938 m, 2878 sh, 1566 w, 1477 m, 1462 sh, 1393 sh, 1372 s, 1267 m, 1190 s, 1082 w, 1030 sh, 988 vs, 926 w, 881 m, 760 s, 633 w, 530 w 469 w cm^{-1}. UV−vis (MeOH, λ_{max}, nm (ϵ)): 224 (7172 ± 50) M^{-1} cm^{-1}. ^1H NMR ($CDCl_3$) δ 1.38 (s, 9H), 8.31 (s, 1H); ^{13}C NMR ($CDCl_3$) δ 82.1, 27.89.

$(CH_3)_3CN(O)NOH$ (2D). This compound is isolated in trace quantities from the reaction of *tert*-butyl bromide and silver hyponitrite. Its spectroscopic properties are identical to those of an authentic sample of *N*-*tert*-butyl-*N*′-hydroxydiazene-*N*-oxide prepared as described below.

To a solution of *N*-*tert*-butylhydroxylamine acetate (1.49 g, 0.01 mol) in aqueous acetic acid (0.1 M, 5 mL) cooled to 0 °C was added a saturated aqueous solution of sodium nitrite (0.695 g, 0.01 mol). The colorless solution was stirred at 0 °C for 2 h, and was allowed to warm to room temperature with stirring overnight. The product formed as yellow globules was extracted with methylene chloride. The methylene chloride solution was dried with anhydrous sodium sulfate. The solvent was removed in a rotary evaporator at room temperature and the product was obtained as yellow liquid. Yield: 0.980 g (83%). Anal. Calcd For $C_4H_{10}N_2O_2$: C, 40.67; H, 8.53; 23.71. Found: C, 40.36; H, 8.38; N, 23.87. IR (cm^{-1}): 2988 s; 2945 m; 1755 w; 1718 w; 1481 s; 1459 s; 1415 s; 1371 vs; 1343 sh; 1248 s; 1187 s; 1071 vs; 1031 m; 946 s; 810 w; 719 s; 674 m; 577 m; 505 w; 426 m. UV−vis (MeOH, λ_{max}, nm (ϵ)): 228 (4710 ± 20) M^{-1} cm^{-1}. ^1H NMR ($CDCl_3$) δ 11.9, N_2O_2H; 1.60, $C(CH_3)_3$; ^{13}C NMR ($CDCl_3$) δ 72.3, $C(CH_3)_3$; δ 27.3, $C(CH_3)_3$.

Synthesis of *tert*-Amylhyponitrite Isomers. These isomers were prepared and separated by the method described above for the *tert*-butyl hyponitrite isomers. *trans*-Di-*O*-*tert*-amylhyponitrite (**3A**) isolated from these isomers has characteristics similar to those reported in the literature.[16,18]

(*Z*)-$C_2H_5(CH_3)_2CN(O)NOC(CH_3)_2C_2H_5$ (3D). Anal. Calcd for $C_{10}H_{22}N_2O_2$: C, 59.37; H, 10.96; N, 13.85%. Found: C, 59.86; H, 10.93; N, 13.56%. IR (Neat): 2978 s, 2940 s, 2884 m, 1481 s, 1467 sh, 1386 m, 1369 m, 1302 w, 1266 w, 1247 w, 1203 w, 1174 m, 1153 sh, 1069 m, 1030 m, 987 vs, 928 w, 841 m, 806 w, 743 w, 740 w, 615 w, 593 w, 563 w cm^{-1}. UV−vis (MeOH, λ_{max}, nm (ϵ)): 234 (6998 ± 60) M^{-1} cm^{-1}. ^1H NMR ($CDCl_3$) δ 1.87 (q, 4H, (CH_3CH_2-C-N), J = 7.43 Hz), 1.73 (q, 4H, (CH_3CH_2-C-O), J = 7.54 Hz), 1.51 (s, 12H, $(CH_3)_2-C-N$), 1.36 (s, 12H, $(CH_3)_2-C-O$), 0.91 (t, 6H, (CH_3CH_2-C-N), J = 7.54 Hz), 0.85 (t, 6H, (CH_3CH_2-C-O), J = 7.48 Hz); ^{13}C NMR ($CDCl_3$) δ 84.7, 76.7, 25.41, 25.40, 33.2, 33.1, 8.51, 8.43.

***trans*-$C_2H_5(CH_3)_2CONNOH$ (4A).** This compound is unstable at ambient temperature and was spectroscopically characterized. IR (neat): 3430 b, 2978 s, 2938 m, 2885 sh, 1561 w, 1462 m, 1372 s, 1301 w, 1248 w, 1210 w, 1174 m, 1152 m, 1083 sh, 1057 m, 989 vs, 932 sh, 874 m, 785 w, 748 w, 631 w, 577 w, 523 w cm^{-1}. UV−vis (MeOH, λ_{max}, nm (ϵ)): 224 (6980 ± 100) M^{-1} cm^{-1}. ^1H NMR ($CDCl_3$) δ 8.03 (s, 1H), 1.34 (s, 6H), 1.70 (q, 2H, J = 7.53 Hz), 0.91(t, 3H, J = 7.52 Hz); ^{13}C NMR ($CDCl_3$) δ 84.4, 25.5, 33.2, 8.36.

$C_2H_5(CH_3)_2CN(O)NOH$ (4D). This compound was isolated in trace quantities and was spectroscopically identified as *N*-*tert*-amyl-*N*′-hydroxydiazene-*N*-oxide. ^1H NMR ($CDCl_3$) δ 12.0 (s, 1H), 1.55 (s, 6H), 1.91 (q, 2H), 0.92 (t, 3H); ^{13}C NMR ($CDCl_3$) δ 75.64, 32.96, 24.74, 8.27.

Synthesis of *p*-$(CH_3)_3CC_6H_4CH_2ONNO$-*p*-$CH_2C_6H_4C(CH_3)_3$ (5A). *p*-*tert*-Butylbenzyl bromide, 1 mL, was dissolved in anhydrous ether and cooled in ice. Excess silver hyponitrite (3 g) was added slowly and the temperature maintained at 0 °C with constant stirring. After the mixture stirred for about 1 h, the precipitated AgBr was filtered off and the solution evaporated under a stream of nitrogen gas. Crystals suitable for X-ray analysis were obtained by recrystallizing the crude product from ether at −68 °C. Yield: 0.73 g, 38%. Anal. Calcd for $C_{22}H_{30}N_2O_2$: C, 74.12; H, 9.05; N, 7.86%. Found: C, 74.11; H, 8.68; N, 7.60%. IR (KBr): 2961 s, 2872 m, 1618 vw, 1516 vw, 1472 w, 1406 vw, 1368 m, 1267 w, 1271 vw, 1113 w, 1013 vs, 936 m, 826 m, 689 w, 565 m cm^{-1}. Raman: 3068 m, 3047 w, 2963 vs, 2954 vs, 2925 m, 2901s, 2863 m, 1611 s, 1508 vw, 1465, w 1441 vw, 1356 w, 1264 vw, 1219 m, 1197 m, 1187 m, 1105 s, 1081s, 1020 vw, 978 vw, 919 w, 854 m, 829 w, 812 s, 745 w, 680 w, 636 m, 623 vs, 542 w cm^{-1}. UV−vis (MeOH, λ_{max}, nm): 226. ^1H NMR ($CDCl_3$) δ 1.32 (s, 18H), 5.23 (s, 4H), 7.31(d, 4H, J = 8.36 Hz), 7.39(d, 4H, J = 8.36 Hz); ^{13}C NMR ($CDCl_3$) δ131.5, 34.8, 75.6, 125. 7, 128. 8, 132.9, 151.8.

Synthesis of $(C_2H_5)_3SiONNOSi(C_2H_5)_3$ (6A). This compound was prepared by the method in **6A** above by the slow addition of 4.00 g of dried silver hyponitrite to 2 mL of chlorotriethylsilane solution in anhydrous ether with constant stirring at 0 °C. (Yield: 1.38 g, 40.7%). Anal. Calcd for $C_{12}H_{30}Si_2N_2O_2$: C, 49.61; H, 10.41%. Found: C, 49.97; H, 10.44. IR (neat): 2959 vs, 2914 s, 2882 s, 1461 m, 1412 m, 1379 w, 1239 m, 1072 m, 1016 sh, 990 vs, 779 s, 742 vs, 681 sh, 579 w, 459 m cm^{-1}. UV−vis (MeOH, λ_{max}, nm (ϵ)): 222 (2522 ± 100) M^{-1} cm^{-1}. ^1H NMR ($CDCl_3$) δ 1.00 (t, 6H, J = 7.82 Hz), 0.79 (q, 4H, J = 7.91 Hz), ^{13}C NMR ($CDCl_3$) δ 7.00, 6.56.

Synthesis of $Tl_2N_2O_2$ (7A). Thallium (I) carbonate was suspended in methanol and cooled in an ice bath. Excess $HClO_4$ was added dropwise until effervescence stopped. The white precipitate of $TlClO_4$ was filtered and dried. Well-dried $TlClO_4$ (1.31 g) was dissolved in water and filtered to remove any insoluble materials. Dried sodium hyponitrite (0.87 g) dissolved in water was added dropwise with constant stirring. The deep yellow precipitate formed was filtered and dried in a vacuum oven at room temperature. Yield: 0.87 g, 47.2%. Anal. Calcd for $Tl_2N_2O_2$: Tl, 87.2; N, 5.97%. Found: Tl, 87.2; N, 5.91%. IR (KBr): 1106 w, 951 vs, 515 w, 499 w, 472 w cm^{-1}. UV−vis (0.1 M NaOH, λ_{max}, nm (ϵ)): 246 (6950 ± 60) M^{-1} cm^{-1}.

Kinetics. The kinetics of the decomposition of *tert*-BuONNOH were performed using a Hewlett-Packard 8452 Diode-Array Spectrometer with quartz cuvettes. The reaction temperature was maintained at 25 °C by means of external circulating baths. The reaction was monitored at 242 nm, and the observed first-order rate constant represents the average of four replicate runs.

Thermal Analysis. Thermal analysis measurements were carried out on a TA Instruments DSC 2010 Differential Scanning Calorimeter equipped with a liquid nitrogen cooling accessory and calibrated with indium reference samples. About 2−5 mg of sample was loaded into an aluminum sample cup for each run. The thermal cycle was performed using 10 °C/min heating rate under an argon atmosphere from 25 to 500 °C. The heat exchanger installed on the DSC cell allows for the measurements of the thermal properties during heating and cooling.

Ab Initio Calculations. The calculations described here were performed using *Gaussian 98* implemented on a Silicon Graphics Iris Indigo workstation.[31] Full optimizations were initially performed at the restricted Hartree−Fock(HF) level using the polarized split valence 6-31G* basis sets before the final optimizations which were performed by density functional theory using Becke's 3 parameter functional and triple split valence basis sets, 6-311++G**.

Crystallographic Structure Determinations. X-ray diffraction data were collected for single crystals of compounds $(CH_3)_3CN(O)NOC(CH_3)_3 \cdot {}^1/_2HONNOH$ (**1D**·$^1/_2$HONNOH), and *p*-$(CH_3)_3CC_6H_4CH_2ONNOCH_2C_6H_4$-*p*-$C(CH_3)_3$ (**5A**) on a Siemens P4 Diffractometer equipped with a molybdenum tube [$\lambda(K\alpha_1)$ = 0.70926 Å; $\lambda(K\alpha_2)$ = 0.71354 Å] and a graphite monochromator at −100 °C. The crystals were mounted on a glass fiber using epoxy adhesive resin and were coated with Paratone N oil. The intensities of three standard reflections were monitored every 100 reflections during the respective data collections indicated negligible crystal decomposition. The structures were solved by direct methods and refined by full-matrix least-squares techniques on F^2 using structure solution programs from the SHELXTL system.[32] Important crystallographic parameters are collected in Table

(31) Frisch, M. J.; Trucks, G. W.; Schlegel, H. B.; Scuseria, G. E.; Robb, M. A.; Cheeseman, J. R.; Zakrzewski, V. G.; Montgomery, J. A., Jr.; Stratmann, R. E.; Burant, J. C.; Dapprich, S.; Millam, J. M.; Daniels, A. D.; Kudin, K. N.; Strain, M. C.; Farkas, O.; Tomasi, J.; Barone, V.; Cossi, M.; Cammi, R.; Mennucci, B.; Pomelli, C.; Adamo, C.; Clifford, S.; Ochterski, J.; Petersson, G. A.; Ayala, P. Y.; Cui, Q.; Morokuma, K.; Malick, D. K.; Rabuck, A. D.; Raghavachari, K.; Foresman, J. B.; Cioslowski, J.; Ortiz, J. V.; Stefanov, B. B.; Liu, G.; Liashenko, A.; Piskorz, P.; Komaromi, I.; Gomperts, R.; Martin, R. L.; Fox, D. J.; Keith, T.; Al-Laham, M. A.; Peng, C. Y.; Nanayakkara, A.; Gonzalez, C.; Challacombe, M.; Gill, P. M. W.; Johnson, B. G.; Chen, W.; Wong, M. W.; Andres, J. L.; Head-Gordon, M.; Replogle, E. S.; Pople, J. A. *Gaussian 98*; Gaussian Inc.: Pittsburgh, PA, 1998.

(32) Sheldrick, G. M. *SHELXTL Crystallograpic System*, version 5.3; Iris Siemens Analytical X-ray Instruments, Inc.: Madison, WI, 1995.

Table 1. Crystallographic Data for **1D·$^1/_2$(HONNOH)** and **5A**

	1D·$^1/_2$(HONNOH)	**5A**
empirical formula	$C_{16}H_{38}N_6O_6$	$C_{22}H_{30}N_2O_2$
fw	410.52	354.48
λ, Å	0.71073	0.71073
space group	$P2_1/c$	$C2/c$
a, Å	7.6869 (6)	13.076 (2)
b, Å	17.979 (2)	10.113 (2)
c, Å	9.0732 (13)	15.780 (2)
α, °	90	90
β, °	92.464(10)	94.146 (8)
γ, °	90	90
V, Å^3	1252.8 (3)	2081.3 (5)
Z	2	4
μ, mm^{-1}	0.083	0.072
ρ_{calcd}, g cm^{-3}	1.088	1.131
T, °C	−100	−100
S_{gof}	1.018	1.049
R_1[a] [$F > 2\sigma F$]	0.0384	0.0463
wR_2[b]	0.1026	0.1169

[a] $R_1 = \Sigma||F_o| - |F_c||/\Sigma|F_o|$. [b] $wR_2 = [\Sigma\{w(F_o^2-F_c^2)^2\}/\Sigma\{w(F_o^2)^2\}]^{1/2}$.

1. Selected atomic positional parameters, interatomic distances and bond angles for **1D** and **5A** are presented in Tables S1−S8 and 2.

$(CH_3)_3CN(O)NOC(CH_3)_3$·$^1/_2$HONNOH (1D·$^1/_2$HONNOH). X-ray diffraction data were collected for a colorless crystal of dimensions, 0.38 × 0.42 × 0.90 mm. The compound crystallizes in the monoclinic space group $P2_1/c$ with 2 $(CH_3)_3CN(O)NOC(CH_3)_3$·$^1/_2$HONNOH in the unit cell, each lying on an inversion center. A total of 2191 (R_{int} = 0.0135) observed independent reflections [$F > 4\sigma(F)$] were collected in the 2θ range, 4.54 to 50°, with the data gathered having $-9 \le h \le 1$, $-21 \le k \le 1$, $-10 \le l \le 10$. The data were not corrected for absorption. All hydrogen atoms were located in successive Fourier maps and refined isotropically, whereas the non-hydrogen atoms were refined anisotropically. The structure was refined by weighted least-squares, $w^{-1} = \sigma^2F_o^2 + (0.0262P)^2 + 0.08P$, where $P = (F_o^2 + 4F_c^2)/3$. The maximum and minimum residual intensities remaining were 0.153 eÅ^{-3} and −0.162 eÅ^{-3}, respectively.

***p*-$(CH_3)_3CC_6H_4CH_2ONNOCH_2C_6H_4$-*p*-$C(CH_3)_3$ (5A).** X-ray diffraction data were collected for a colorless crystal of dimensions, 0.5 mm × 0.62 mm × 0.74 mm. The compound crystallizes in the monoclinic space group $C2/c$ with four *p*-$(CH_3)_3CC_6H_4CH_2ONNO$-*p*-$CH_2C_6H_4C(CH_3)_3$ molecules in the unit cell, each located on a center of inversion. A total of 1821 (R_{int} = 0.0225) observed independent reflections [$F > 4\sigma(F)$] were collected in the 2θ range, 5.10 to 50°, with the data gathered having $-1 \le h \le 15$, $-12 \le k \le 1$, $-18 \le l \le 18$. The data were not corrected for absorption. All hydrogen atoms were located in successive Fourier maps and refined isotropically, whereas the non-hydrogen atoms were refined anisotropically. The structure was refined by weighted least-squares, $w^{-1} = \sigma^2F_o^2 + (0.0763P)^2 + 4.54P$, where $P = (F_o^2 + 4F_c^2)/3$. The maximum and minimum residuals in the electron density difference maps were 0.285 eÅ^{-3} and −0.217 eÅ^{-3}, respectively.

Results

Synthesis. The alkylation reactions of silver hyponitrite were carried out by the procedure of Kiefer et al.[15] When silver hyponitrite was added to a solution of *tert*-butyl bromide at ∼0 °C, a vigorous effervescence with the evolution of a colorless gas was observed. The yields for these reactions were generally low. As shown in the Scheme 1 and Table 3 below, four products were isolated from the reactions of *tert*-butyl and *tert*-amyl bromide with silver hyponitrite. The ratio of the products was only slightly altered by the addition of K_2CO_3 to the reaction mixture. Together with that of the four isomers the formation of the corresponding alcohols was also observed. When substoichiometric amounts of *tert*-butyl bromide or *tert*-amyl bromide were used in the reactions, the *trans*-mono-O-alkylated isomer was obtained as the predominant product.

However, in the reaction of *p*-*tert*-butylbenzyl bromide with silver hyponitrite, *trans*-di-O-alkylated hyponitrite was isolated as the sole alkylated product together with small amounts of *p*-*tert*-butylbenzyl alcohol and *p*-*tert*-butylbenzyl aldehyde. Similarly, only the *trans*-di-*O*-silyl hyponitrite was isolated in good yield (Table 3) from the reaction of chlorotriethylsilane with silver hyponitrite.

Alkylation reactions of $Na_2N_2O_2$, $Tl_2N_2O_2$, $[HEt_2NCH_2CH_2NEt_2H][N_2O_2]$,[19] and $[quinuclidinium]_2[N_2O_2]$[19] were also attempted by treating ethereal solutions of the alkyl halides with the corresponding hyponitrite salts. However, the reactions did not yield alkylated products.

During the separation of the constitutional isomers present in the mixture of products obtained from the reaction of *tert*-butyl bromide with silver hyponitrite, *trans*-mono-*O*-*tert*-butyl hyponitrous acid was found to decompose slowly on silica gel and rapidly on alumina to *tert*-butyl alcohol and nitrous oxide. Although the isomers were separated by chromatographic techniques, pure *trans*-di-*O*-*tert*-butyl hyponitrite could also be obtained by re-crystallizing the crude mixture from methanol at −58 °C as reported in the literature.[15] Pure crystals of (*Z*)-*N*-*tert*-butyl-*N*′-*tert*-butoxydiazene-*N*-oxide, as its hyponitrous acid adduct, could also be obtained by subjecting the crude product mixture to high vacuum; the more volatile components are removed leaving behind only (*Z*)-*N*-*tert*-butyl-*N*′-*tert*-butoxydiazene-*N*-oxide with solvated hyponitrous acid (**1D**·$^1/_2$HONNOH). The remaining two isomers were separated by column chromatography or by preparative TLC plates as described in the Experimental Section.

Kinetics. The decomposition of *tert*-BuONNOH in 1.0 M NaOH, ionic strength (I = 1.0 M) at 25 °C, results in the formation of *tert*-BuOH and N_2O, respectively, according to the eq 1. The rate law for the decomposition of *tert*-BuONNOH is given by eq 2 with a first-order rate constant (k) of (1.08 ± 0.01) × 10^{-3} s^{-1}.

$$t\text{-BuONNOH} + OH^- \xrightarrow{k} t\text{-BuOH} + N_2O\uparrow \qquad (1)$$

$$-d[t\text{-BuONNO}^-]/dt = k[t\text{-BuONNO}^-] \qquad (2)$$

Spectroscopic Results. The IR spectra of these compounds were recorded between 4000 and 400 cm^{-1}. The spectra exhibit a strong peak at ∼1000 cm^{-1} corresponding to the N−O asymmetric stretch vibrational mode. In addition, the spectra of compounds **2A** and **3A** also exhibit a peak in the 3400 cm^{-1} region indicating the presence of hydroxyl group together with another absorption at ca. 1540 cm^{-1} corresponding to δ(OH) stretching vibrational mode (Table 4).

The UV−visible spectra for the compounds were measured at room temperature in methanol solution. The spectral data are collected in Table 4. The spectra of compounds **1A**, **2A**, **3A**, **4A**, **5A**, and **6A** exhibit single bands with λ_{max} in the narrow 224−226 nm region while compounds **1D** and **3D** exhibit a single band at λ_{max} 234 nm.

Differential Scanning Calorimetric Data. The thermal decomposition properties of compounds **1A**−**7A**, **1D**, and **3D** were studied by differential scanning calorimetry in the temperature region, 25−500 °C, under a steady stream of argon gas. Compounds **1A**−**7A** undergo exothermic decomposition, while compounds **1D** and **3D** undergo endothermic decomposition, and the data are presented in Table 5.

Theoretical Results. Optimized ground-state structures calculated for *trans*-dimethylhyponitrite, **8**, *trans*-methylhyponitrite, **9**, (*Z*)-*N*-methyl-*N*′-methoxydiazene-*N*-oxide, **10**, and *N*-

Table 2. Selected Bond Lengths (Å) and Angles (deg) of **1D·$^1/_2$(HONNOH)** and **5A**

compds	N═N (Å)	N−O (Å)	N−N−O (deg)	other parameters
1D·$^1/_2$(HONNOH)	N(1)−N(2) 1.264 (2)	N(1)−O(1) 1.2679 (14)	N(1)−N(2)−O(2) 108.66 (10)	C(1)−O(2) 1.483 (2) (Å)
		N(2)−O(2) 1.369 (2)	N(2)−N(1)−O(1) 125.47 (11)	O(1)···O(3) 2.696 (2) (Å)
	N(3)−N(3A) 1.216 (2)	N(3)−O(3) 1.382 (2)	N(3)−N(3A)−O(3) 108.22 (14)	O(1)−N(1)−C(5) 117.65 (10) (°)
				N(2)−O(2)−C(1) 109.67 (10) (°)
				O(2)−C(1)−C(2) 109.31 (13) (°)
				O(2)−C(1)−C(3) 109.13 (12) (°)
				O(2)−C(1)−C(4) 101.83 (13) (°)
5A	N(1)−N(1A) 1.230 (3)	N(1)−O(1) 1.361(2)	N(1)−N(1A)−O(1) 107.7 (2)	C(1)−O(1) 1.468 (2) (Å)
				N(1)−O(1)−C(1) 108.29 (13) (°)
				O(1)−C(1)−C(2) 108.0 (2) (°)

Scheme 1. Reaction of *tert*-Butyl- or *tert*-Amyl Bromides with $Ag_2N_2O_2$

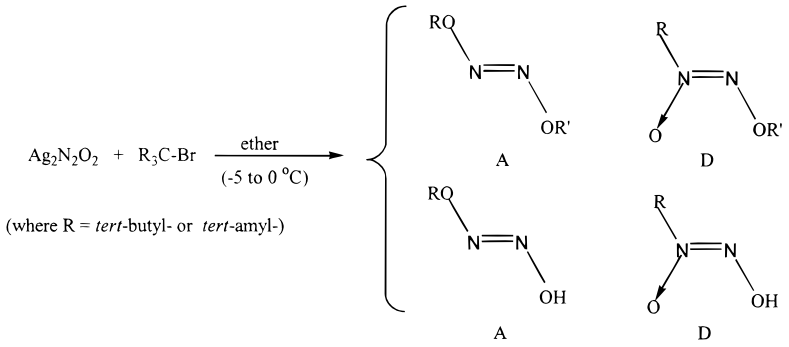

R	$(CH_3)_3C$	$(CH_3)_3C$	$C_2H_5(CH_3)_2C$	$C_2H_5(CH_3)_2C$	*p*-$(CH_3)_3CC_6H_4CH_2$	$(C_2H_5)_3Si$
R'	$(CH_3)_3C$	H	$C_2H_5(CH_3)_2C$	H	*p*-$(CH_3)_3CC_6H_4CH_2$	$(C_2H_5)_3Si$
No.	**1**	**2**	**3**	**4**	**5**	**6**

Table 3. Reactions of Alkyl Halides with Silver Hyponitrite[a]

alkyl group (R)	reaction conditions	mole ratio of RBr to $Ag_2N_2O_2$	order of addition	isolated yield (%) ± 1%				
				RONNOR	RN(O)NOR	RONNOH	RN(O)NOH	Total
$(CH_3)_3C$	Et_2O	2:1	$Ag_2N_2O_2$ to RBr	16	6	8	2	32[d]
$(CH_3)_3C$[b]	Et_2O/K_2CO_3	3:1	$Ag_2N_2O_2$ to RBr	12	6	13	2	33[d]
$(CH_3)_3C$[c]	Et_2O	1:1	RBr to $Ag_2N_2O_2$	6	4	18	4	32[d]
$CH_3CH_2(CH_3)_2C$	Et_2O	2:1	$Ag_2N_2O_2$ to RBr	14	8	7	2	31[d]
[b]$CH_3CH_2(CH_3)_2C$	Et_2O/K_2CO_3	2:1	$Ag_2N_2O_2$ to RBr	11	5	12	1	29[d]
[c]$CH_3CH_2(CH_3)_2C$	Et_2O	1:1	RBr to $Ag_2N_2O_2$	7	4	16	3	30[d]
p-$(CH_3)_3CC_6H_4CH_2$	Et_2O	1:2	$Ag_2N_2O_2$ to RBr	38	*e*	*e*	*e*	38[d]
$(CH_3CH_2)_3Si$	Et_2O	1:1.5	$Ag_2N_2O_2$ to RBr	41	*e*	*e*	*e*	41[d]

[a] All reactions were performed in ~20 mL ether at −5 to 0 °C for 45 min except the last reaction that performed for about 24 h. [b] These reactions were performed in ~20 mL ether/K_2CO_3. [c] A substoichiometric equivalent of the corresponding alkyl halides was added to an ether suspension of excess $Ag_2N_2O_2$. [d] The yield was estimated from the ^{1}H NMR integration ratio and the actual yield. [e] Products not formed.

methyldiazenenium diolate, **11**, at B3LYP/6-311++G** level of theory are shown in Figure 5. The local minima for all four structures have a mirror plane of symmetry defined by the ONNO framework. The *trans* derivative **8** has inversion and C_2 axial symmetries, which result in a net C_{2h} point group symmetry. Thus for their respective point groups the vibrations of **8**, C_s, symmetry, are either in plane, A′, or out of plane, A″, while for **9**, C_{2h} point symmetry, these modes are either gerade or ungerade with respect to the inversion symmetry. At the B3LYP/6-311+G* level of theory optimization of the *trans*-hyponitrite dianion has N−O and N═N bond lengths of 1.3671 and 1.2645 Å, respectively, and an O−N−N bond angle of 115.421° Comprehensive lists of the vibrational modes, their energies, and symmetries are collected in Table S9.

Structural Data. Compounds **1D·$^1/_2$**HONNOH and **5A** have been characterized by single X-ray diffraction data at −100 °C. Selected bond distances and angles are presented in Table 2.

Structure of $(CH_3)_3CN(O)NOC(CH_3)_3$·$^1/_2$HONNOH (1D·$^1/_2$HONNOH). The crystals contain *N*-*tert*-butyl-*N*′-*tert*-butoxydiazene-*N*-oxide (**1D**) cocrystallized with hyponitrous acid as shown in Figure 2. Whereas the diazene-*N*-oxide molecule occupies general positions, the hyponitrous acid molecule lies on an inversion center. All atoms of the latter molecule are coplanar, and the molecule possesses *trans* geometry. Bonding features associated with the acid molecule are comparable to those of the molecule also present as solvate in the crystals of the *N*, *N*-*N*′, *N*′-tetraethylethylenediammonium salt of hyponitrous acid.[19]

The N_2O_2 fragment in the diazene-*N*-oxide exhibits Z geometry with respect to the orientation of the *N*-oxide and *tert*-butoxy oxygen atoms. The fragment is nearly coplanar with the maximum deviation from the least mean squares plane being 0.0017 Å and the dihedral angle between the two NNO planes being 0.6°. The bonding environment of one of the two nitrogen

Table 4. Spectroscopic Results for New Compounds

	IR				UV−vis (in MeOH)	
compound	ν(OH)	δ(OH)	ν(N−O)$_{as}$	other bands[f]	$\lambda_{(max)}$	$\epsilon_{(max)}$ (M^{-1} cm^{-1})
1A			995[a]		226[a]	6200[a]
			990[b]		224.6[b]	7010[b]
			995[c] vs		226[c]	7100[c]
1D		-	1061 vs	ν(N═N) 1485 s	234	7200
			991 s			
1D·$^1/_2$(HONNOH)	3207 b	1532 m	1067 vs	ν(N═N) 1485 s		
				1004 vs		
				991 vs		
2A	3418 b	1566 w		988 vs	224	7172
2D		1718 w	1071 vs	ν(N═N) 1481 s	228	4710
3A			990[b] vs		225[b]	7000[b]
			988[c] vs		226[c]	7060[c]
3D	-	-	1069 s	ν(N═N) 1481 s	234	6998
4A	3430 b	1561 w	989 vs		224	6980
5A	-		1013 vs	ν(N−N)$_{as}$ (Ram) 1611 s	226[d]	-
				ν(N−O)$_s$ (Ram) 1081 s		
				ν(N−N−O)$_s$ (Ram) 623 vs		
6A	-		990 vs		222	2522
7A	-		951 vs		246[e]	6950[e]

[a] Reference 15. [b] Reference 18. [c] This work. [d] Benzyl chromophore overlap prevents quatitative determination of ϵ. [e] 0.1 M NaOH. [f] Raman active bands denoted (Ram).

Table 5. Differential Scanning Calorimetric Data

compound	T_{onset} (°C)	T_{max} (°C)	ΔH (cal/g)	ΔH (kcal/mol)
1A	-	82[a]	-	-
1A	-	84.5[b]	-	-
1A	86.5[c]	91.4[c]	−62.3[c]	−10.84[c]
1D	86.7	119	+37.4	+6.52
1D·$^1/_2$(HONNOH)	76.5	81.2	+34.8	+16.72
	120	142	+35.9	
2A	73.4	90.8	−55.4	−6.55
2D	66.4	68.3	−7.59	−0.897
3A	73.9	92.7	−131	−26.46
3D	106	136	+40.3	+8.15
4A	81.0	93.3	−57.3	−7.52
5A	74.7	84.1	−198	−71.67
6A	117	143	−150	−33.65
7A	190	205	−51.1	−23.93

[a] Reference 15. [b] Reference 30. [c] This work.

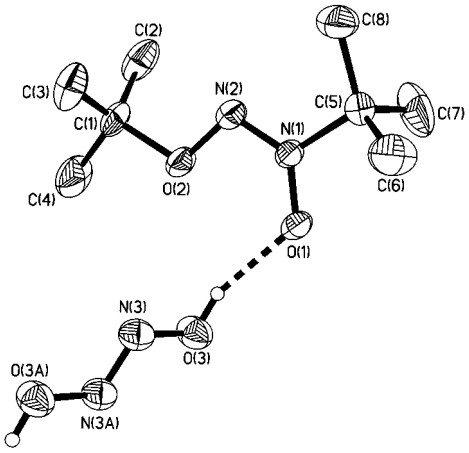

Figure 2. ORTEP view of $(CH_3)_3CN(O)NOC(CH_3)_3 \cdot {}^1/_2(HONNOH)$. All atoms except hydrogen atoms are labeled.

atoms, N(1), is trigonal planar (sum of bond angles = 360°). The observed N−N, N−O_{butoxy}, N−O_{oxide} bond distances of 1.264(1) Å, 1.369(1) Å, and 1.268(1) Å, respectively, indicate delocalized π-bonding over the N_2O_2 fragment. Four other compounds, namely, *N*-methyl-*N*′-methoxydiazene-*N*-oxide,[24] methylene-bis(*N*′-methoxydiazene-*N*-oxide),[23] ethane-1,1-bis(*N*′-methoxydiazene-*N*-oxide), and propane-2,2-bis(*N*′-methoxydiazene-*N*-oxide)[25] also exhibit similar structural features.

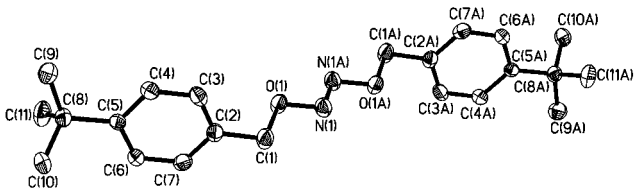

Figure 3. ORTEP view of $(CH_3)_3CC_6H_4CH_2ONNOCH_2C_6H_4C(CH_3)_3$. All atoms except hydrogen atoms are labeled.

The diazene-*N*-oxide and hyponitrous acid molecules are involved in intermolecular hydrogen bonding. The two symmetrically related hydroxy groups of the acid molecule interact with the *N*-oxide oxygen atoms of two diazene-*N*-oxide molecules with the O···O distance of 2.696(2) Å.

Structure of *p*-$(CH_3)_3CC_6H_4CH_2ONNOCH_2C_6H_4$-*p*-C-$(CH_3)_3$ (5A). The structure consists of *trans*-*p*-di-*tert*-butylbenzyl hyponitrite molecules, with the N═N bond situated on an inversion center, Figure 3. The molecule exhibits *trans* geometry with respect to the orientation of the two alkoxy groups, and the N_2O_2 fragment is planar similar to *trans*-di-*O*-*tert*-butyl hyponitrite.[17] However, the observed N−N, N−O, and O−C bond distances of 1.230(3) Å, 1.361(2) Å, and 1.468(2) Å, respectively, are significantly shorter (∼0.02 Å) in comparison to those in *trans*-di-*O*-*tert*-butyl hyponitrite.[17]

Discussion

A critical observation described here is that the reaction of *tert*-butyl- and *tert*-amyl bromides with $Ag_2N_2O_2$ leads to ambiphilic alkylation of $Ag_2N_2O_2$. Of the oxyanions of nitrogen the best understood ambiphilic alkylation is for the reaction of *tert*-butyl- and *tert*-amyl halides with silver nitrite which results in both the nitrito and nitro derivatives.[3−5] Although the ambiphilic alkylation of silver hyponitrite with bromo- and chlorodiphenylmethane has been outlined,[6] this report describes this reactivity pattern for a wider range of electrophiles. Curiously, despite the numerous experiments with di-*tert*-butyl hyponitrite it is the only reported product from the alkylation of silver hyponitrite with *tert*-butylbromide. The most plausible

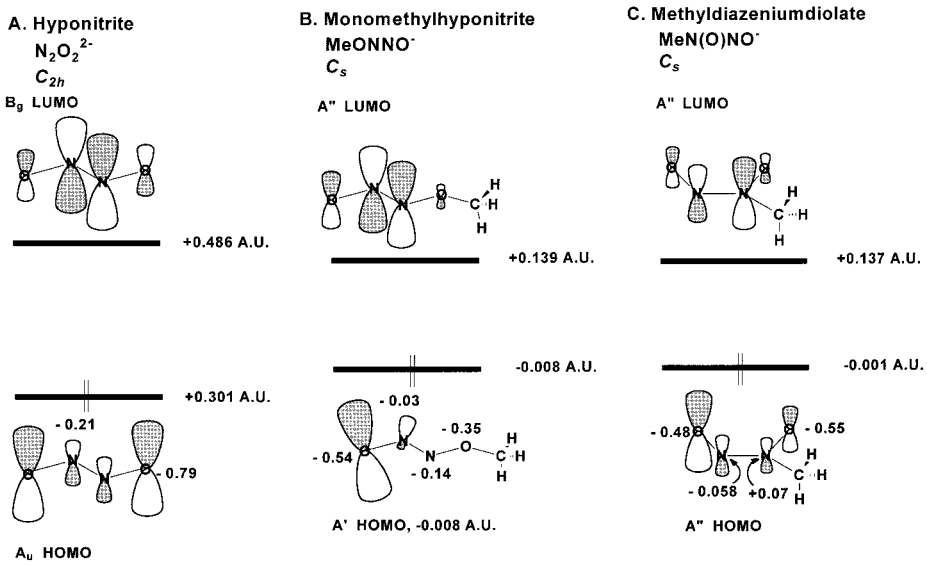

Figure 4. Frontier molecular orbital diagrams and Mulliken charges for $N_2O_2^{2-}$, $MeONNO^-$, and $MeN(O)NO^-$.

reason other workers have not observed the formation of the complete product spectrum in the alkylation of hyponitrite is due to the routine use of methanol in the final recrystallization step. This step allows for the isolation and separation of compound **A** from all of the other products.[15] Unlike *trans*-di-*O*-alkyl hyponitrite, the polar O/N-alkylated products, as well as the mono-alkylated products, are highly soluble in methanol and water.

To help understand the regioselectivity in these alkylation reactions we have performed ab initio calculations for *trans*-hyponitrite, *trans*-hyponitrous acid, analogues of the most likely intermediates in these reactions, and representative S_N2 transition states corresponding to O- and N-alkylation. For computational efficiency we have optimized the geometries and calculated the frequencies for the mono- and dimethyl analogues of these species with density functional theory, B3LYP, and large basis sets, 6-311++G**, Figure 5. The HOMO and LUMO orbitals for mono-*O*-alkyl and mono-*N*-alkyl hyponitrite anions are shown in Figure 4. The HOMO of the hyponitrite dianion has A_u symmetry and is delocalized over the complete framework. However, the Mulliken charges and the orbital coefficients indicate slightly more electron density resides on the oxygens than the nitrogens, both being critical factors for a limiting S_N1 alkylation mechanism. The other limiting case is an S_N2 transition state where C−O or C−N bond formation is coupled to C−X bond cleavage. To help distinguish between oxygen and nitrogen nucleophilicity in O vs N alkylation we have calculated the transition states for the addition of methyl chloride to either atom. The geometries for these transition states, shown in Figure 6, were initially located by scanning the energies of Z-matrix representations of the expected transition state with respect to the Cl−C−H angle as a function of the reaction coordinate. The resulting initial transition states were subsequently completely optimized to give the transition-state structures in Figure 6. Confirmation that these transition states connect the reactants, $MeONNO^-$ and CH_3Cl, with the products, MeONNOMe or MeONN(O)Me and Cl^-, was found by geometrical optimization of the steps along the internal reaction coordinate away from the transition-state saddle point. As shown in Figure 6 alkylation of either oxygen or nitrogen with methyl chloride gives slightly early transition states characterized by an O−C−H and an N−C−H angles of 84.53° and 87.88°, and which have $\Delta E_a^{\ddagger}$ of 5.6 and 7.5 kcal mol^{-1}, respectively.

Any discussion of the mechanism of hyponitrite alkylation is tempered by the heterogeneous nature of these transformations and the concomitant absence of homogeneous phase kinetic data (see below). There is also a critical requirement for a Lewis acid, in our experiments the silver cation, and this poses the possibility for electron-transfer catalysis in these alkylations.[33] Despite these severe limitations, we note that Mendenhall has concluded that the reactivity of alkyl halides with $Ag_2N_2O_2$ follows the stability of the incipient carbocation,[6] and thus there is likely to be considerable S_N1 character in these transition states. In his seminal studies of the ambident alkylation of nitrite Kornblum dissected these alkylations into transition states with varying S_N1/S_N2 character.[3,4] Many of his conclusions can be more succinctly stated in terms of frontier molecular orbital theory,[34] and we note that very complicated ambident nucleophilicity can be successfully understood in terms of charge vs orbital control as well by considerations of thermodynamic/kinetic control.[35,36]

Initial O-alkylation results in a mono-*O*-alkyl hyponitrite intermediate species, $RONNO^-$. As can be seen in Figure 4, the Mulliken charges of $MeONNO^-$ are more biased toward the nonalkylated oxygen atom, and the HOMO is largely localized on this same atom. The expectation for either a charge or orbital controlled reaction, for the S_N1 limiting case, is then for the second alkylation to occur by attack of the incipient carbocation on the oxygen atom, resulting in the formation of *trans*-di-*O*-alkyl hyponitrite, RONNOR, as the major product, as found for the entries in Table 3 for R = Et_3Si, *p*-$(CH_3)_3CC_6H_4CH_2$, and $(CH_3)_3C$. In the first two cases the O/O-dialkylated product is the only one isolated. Since charge and orbital localization on the nitrogen atom of the nonalkylated half of the species is very poor, N-alkylation will be highly disfavored. In the case of a limiting S_N2 mechanism the gas-phase transition states for the alkylation of $MeONNO^-$, Figure 6, also suggest that the comparatively low barriers to O-alkylation will favor the formation of MeONNOMe. Therefore,

(33) Kornblum, N. *Chemistry of the Amino, Nitroso, and Nitro Functional Groups*; Patai, S., Ed.; Wiley: New York, 1982; Part I, Suppl. F, Chapter 10, pp 361−393.

(34) Fleming, I. *Frontier Orbitals and Organic Chemical Reactions*; Wiley & Sons: London, 1976.

(35) Arndt, A.; Handke, G.; Krause, N. *Chem. Ber.* **1993**, *126*, 251−259.

(36) Frederick, M. A.; Hulce, M. *Tetrahedron* **1997**, *53*, 10197−10227.

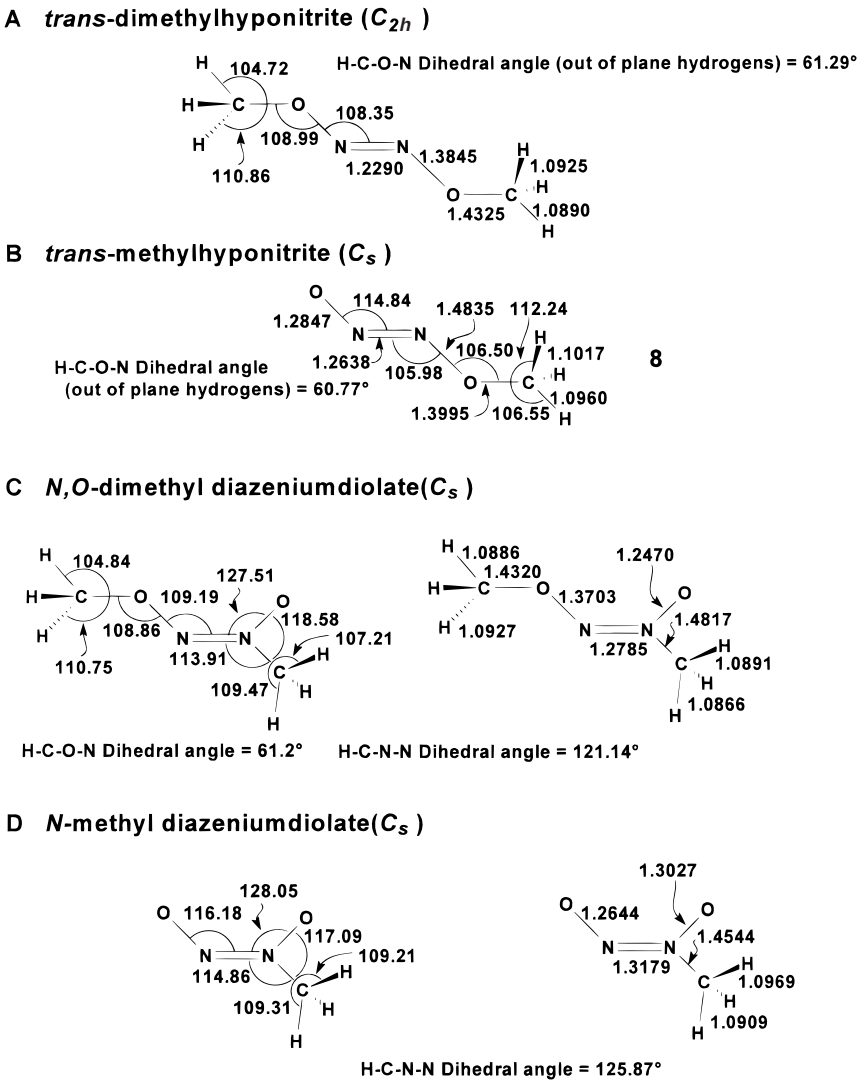

Figure 5. Optimized ground-state structures of critical substrates and proposed intermediates in this study. Geometries calculated at B3LYP/6-311++G** level of theory, distances given in Å and angles given in degrees.

the formation of (*Z*)-*N*-alkyl-*N*′-alkoxydiazene-*N*-oxide species **D** probably does not involve the mono-O-alkylated intermediate.

The formation of (*Z*)-*N*-alkyl-*N*′-alkoxydiazene-*N*-oxide from *trans*- or (*E*)-hyponitrite can be rationalized as follows. The first alkylation could occur on one of the two nitrogen atoms resulting in the formation of a mono-*N*-alkylhyponitrite or diazenium diolate species, $RN(O)NO^-$. As can be seen in Figure 4, the Mulliken charges and the orbital coefficients of the HOMO of $MeN(O)NO^-$ are significantly localized on the second oxygen atom, suggesting that in an S_N1 limiting mechanism O-alkylation of the terminal oxygen will be more favored over second N-alkylation.

The experimental observation of the formation of *trans*-di-*O*-alkylhyponitrite and *N*-alkyl-*N*′-alkoxydiazene-*N*-oxide, with the former being the major product, is consistent with the above theoretical arguments. The isolation of the two protonated species of the initial mono-O- and mono-N-alkyl derivatives, namely, mono-*O*-*tert*-butylhyponitrous acid, $(CH_3)_3CONNOH$, and *N*-*tert*-butyl-*N*′-hydroxydiazene-*N*-oxide, $(CH_3)_3CN(O)NOH$, also supports the above arguments. However, the observed Z-geometry for *N*-*tert*-butyl-*N*′-*tert*-butoxydiazene-*N*-oxide remains to be explained.

On the basis of the frontier molecular orbital calculations and model transition states we predict that initial O-alkylation does not lead to mixed N/O-dialkylated products. It is however instructive to consider the sequence of events that might follow from subsequent *trans/cis* or E/Z-isomerization after O-alkylation. If initial O-alkylation forms the *trans*-mono-O-alkylated intermediate, isomerization of the *trans*-O-alkylated intermediate to the Z form might occur before the second N-alkylation. However, we have found that the Z form of the O-alkylated intermediate is electronically unstable; at both the B3LYP and MP2 levels of theory we are unable to find a stable minimum which would correspond to *cis*-*O*-monomethyl hyponitrite, **G** in Figure 7. All attempts to locate such a minimum consistently optimize to a weakly associated methoxide adduct of nitrous oxide, Figure 7, as the local minima. Thus, the potential energy surface which describes the reaction coordinate between the putative structure **G**, and the minimum in Figure 6, does not contain a significant barrier which would result in a saddle point/transition state. Therefore, *trans* → *cis*, or E → Z, isomerization is expected to spontaneously result in the formation of RO^- and nitrous oxide, and this may account for why *cis*-dialkylated hyponitrites are not isolated in these reactions. Also, a second N-alkylation of the *trans*-$RONNO^-$ is electronically disfavored. We conclude that the formation of N/O-dialkyl products most likely occurs via the mono-N-alkylated intermediate species. A comparison of the ground-state energies of the E and Z forms of the *N*/*O*-dialkyl hyponitrite indicates that the Z form is marginally more thermodynamically stable, ~2 kcal/mol, in the

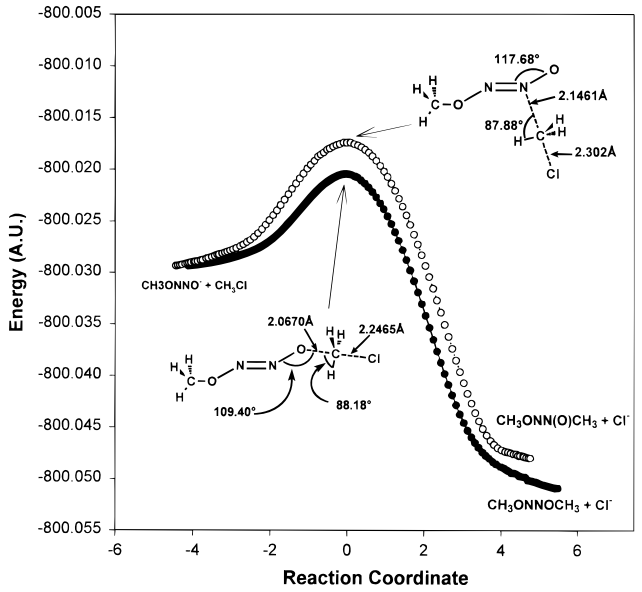

Figure 6. Transition-state structures and reaction paths for alkylation of $MeONNO^-$ at the oxygen, filled circles, and the nitrogen, open circles. Theory and basis set: B3LYP/6-311++G**.

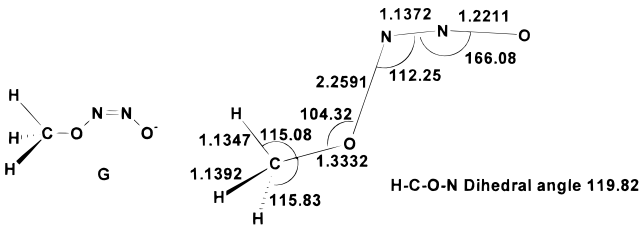

Figure 7. Proposed and optimized ground-state structures for the putative *cis-mono*-methyl hyponitrite, $MeONNO^-$. Note that the minimized structure on the right corresponds to a methoxy adduct of nitrous oxide rather than to a configurational isomer of **8** in Figure 5.

gas phase and is separated from the E-form by a low barrier of 9 kcal/mol.[26] Therefore, the initially formed E isomer can be expected to undergo isomerization to the Z-form.

In support of the argument that only initial N-alkylation pathway leads to N/O-dialkylated product, we note that the alkylation of the silver salt of (*Z*)-*N*-*tert*-butyl-*N*′-hydroxydiazene-*N*-oxide with *tert*-butyl bromide yields only the N/O-dialkylated product, **1D**. This suggests that the oxygen site is the most favored in the second alkylation step, and that the intermediacy of species such as **2D** or **4D** result in the formation of **1D** and **3D.** If the substrate possesses two sites with unequal charge localization as in the hyponitrite anion, the nature of the cation, its size, stability, and charge localization determine whether the cation will attack one or both of the sites. The cations generated from *p*-*tert*-butylbenzyl bromide and chlorotriethylsilane exclusively attack the more negatively charged oxygen atoms of the hyponitrite anion, and therefore no formation of other products is observed.

The mechanism of the alkylation reactions of silver hyponitrite with *tert*-butyl bromide and *tert*-amyl bromide is summarized in Scheme 2. The first pathway involves the initial alkylation of one of the two oxygen atoms of hyponitrite dianion to form the *trans*-mono-*O*-alkyl hyponitrite intermediate species, which may be further alkylated or protonated to form the corresponding *trans*-di-*O*-alkyl hyponitrite (**1A** and **3A**) and *trans*-mono-O-alkylated hyponitrite (**2A** and **4A**), respectively. The second pathway involves the initial alkylation of one of the two nitrogen atoms to form the unstable (*E*)-*N*-alkyl intermediate, which would then have to undergo E/Z isomerization to form the comparatively more stable Z form of the intermediate. This intermediate would then undergo a second O-alkylation (**1D** and **3D**) or O-protonation (**2D** and **4D**) to give the observed products. Due to either their inherent instability, or to the conformational dynamics leading to their formation, compounds with the structure **B**, **C**, **E**, and **F**, were not observed in any of the alkylation reactions studied.

To help understand the origin of protons and protonated mono-alkylated derivatives in these reactions, a NMR experiment was carried out in dry C_6D_6 using *tert*-amyl bromide and $Ag_2N_2O_2$. The spectrum exhibits the characteristic peaks at 5.2 (quintet) and 4.8 (singlet) ppm corresponding to the methyne proton of the 2-methyl-2-butene, and the methylene protons of 2-methyl-1-butene, respectively, together with peaks corresponding to the alkylated products. The two butenes result from E2 elimination from the alkyl bromide. As shown in Table 3 addition of solid-phase potassium carbonate to the reaction has little effect on either the product distribution or the yield of the reaction. Similar elimination reactions have also been reported for the reaction of cyclohexyl bromide with $Ag_2N_2O_2$.[6] Also, from these NMR results, the colorless gas observed during the reaction of *tert*-butyl bromide with silver hyponitrite may be ascribed to the formation of 2-methylpropene $\{CH_2{=}C(CH_3)_2\}$ which has a boiling point at −6.9 °C. The observed instability of *trans*-mono-*O*-alkyl hyponitrite in basic conditions is consistent with the reported instability of mono protonated hyponitrous acid ($HONNO^-$) in the 8−10 pH range.[8] Attempts to alkylate *trans*-mono-*O*-*tert*-butylhyponitrous acid with diazomethane in ether were unsuccessful, as were attempts to isolate the corresponding silver salt. All of these observations can be attributed to the ease of elimination of alkoxide (or hydroxide) from $RONNO^-$ with the concomitant formation of nitrous oxide. This deleterious reaction may also account for the uniformly low overall yields from these reactions.

Sodium nitrite is readily alkylated with alkyl halides at ambient temperatures in DMSO or DMF.[4] However, the alkylation of $[HEt_2NCH_2CH_2NEt_2H][N_2O_2]$,[19] $[quinuclidinium]_2[N_2O_2]$,[19] $Na_2N_2O_2$, or $Tl_2N_2O_2$ in DMSO, DMF, or ether with *tert*-butyl bromide or *p*-*tert*-butylbenzyl bromide were all unsuccessful. We concur with Mendenhall's prior results which demonstrated that Lewis acids are required to promote these alkylation reactions,[6,37] and that in certain heterogeneous conditions, for example, ferric chloride or zinc chloride suspensions in ether or pentane, the yield of *O*/*O*-dialkylhyponitrite can be quite high, > 85%. Unfortunately the kinetics of these reactions are difficult to determine due the heterogeneous conditions, the thermal instability, and general insolubility of most simple hyponitrite salts. As described above, the markedly more soluble bis-tetraalkylammonium salts of hyponitrite are not alkylated under these conditions either, even in polar organic solvents such as DMSO, DMA, or DMF. Surprisingly, thallium hyponitrite is not alkylated under these conditions either, even though TlBr and AgBr have similar solubilities. Ultimately, the silver and other Lewis acids may have the role originally ascribed to it by Kornblum, that is, the silver ion polarizes the carbon−halogen bond of the alkyl halides, which consequently stabilizes the transition state through interaction with the leaving group.[4]

The structural results for **1D**·$^1/_2$HONNOH and **5A** not only confirm the stereochemistry of the product, but they also allow for considerable insight into the electronic structures for these species. Of particular note the lattice cocrystallized hyponitrous acid in **1D**·$^1/_2$HONNOH is required for crystallization of **1D**;

(37) Mendenhall, G. D. *Tetrahedron Lett.* **1983**, *24*, 451−452.

Scheme 2. Proposed Mechanism for O,N-Alkylation of $Ag_2N_2O_2$

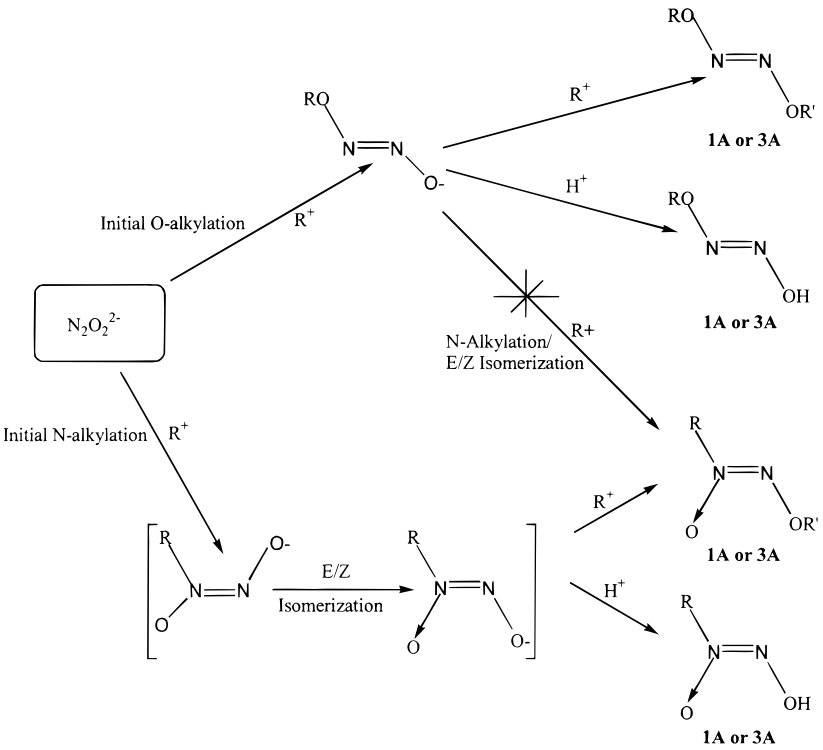

pure **1D** is an oily liquid at room temperature. This is only the second reported instance of a structurally characterized cocrystallized hyponitrous acid, the other being in $[HEt_2NCH_2CH_2NEt_2H][HONNO]_2 \cdot HONNOH$, **12A**.[19] In both cases the metric parameters are similar, N═N 1.226(4) and 1.216(2) Å, N−O 1.363(3) and 1.382(2) Å, N−N−O 109.9(3) and 108.22(14)°, in **12A** and **1D** respectively. Theoretically calculated gas-phase ground-state values for these parameters, B3LYP/6-311++G**, are in very good agreement with these crystallographic data: N═N 1.2254, N−O 1.3885 Å, and N−N−O 108.231°. The hyponitrous acid is of course hydrogen-bonded in both solid-state structures, resulting in O−O separations of 2.648(3) and 2.696(2) Å in **12A** and **1D** respectively. Supporting evidence for this is also found in the IR spectra which have broad ν(O−H−O) bands at 3177 and 3207 cm^{-1} in **12A** and **1D** respectively. In contrast, the theoretically calculated ν(O−H) vibrational bands (B3LYP/6-311++G**) are much higher for gas-phase hyponitrous acid occurring at 3816.41 and 3813.49 cm^{-1} for the A_g and B_u modes, respectively.

The diazenium diolate portion of the structure of **1D** indicates that this species adopts a Z geometry with metrical parameters very similar to those reported for the related compounds *N*-methyl-*N*′-methoxydiazene-*N*-oxide,[24] methylene-bis(*N*′-methoxydiazene-*N*-oxide),[23] ethane-1,1-bis(*N*′-methoxydiazene-*N*-oxide),[25] and propane-2,2-bis(*N*′-methoxydiazene-*N*-oxide).[25] In all of these structures the N═N bond lengths are longer than those found for the hyponitrous acid cocrystallite and for dialkylhyponitrites. In **1D**, the N(1)−O(1) and N(2)−O(2) bond lengths, 1.369 (2) Å and 1.2679 (14) Å, are both significantly shorter than the N−O bond lengths in hyponitrous acid and **5A**. These observations are consistent with π-bond delocalization over the N(1)−N(2)−O(2) framework. These metric parameters are similar to those calculated for the bis-dimethyl analogue, *N*-methyl-*N*′-methoxydiazene-*N*-oxide (Figure 5). Together these experimental and theoretical results suggest that the shortening of the N(2)−O(2) bond is consistent with multiple bonding or π-delocalization which in turn is found in azine-*N*-oxides. From this perspective a diazenium diolate such as **1D** is the *N*-oxide of the unknown O-alkylated diazotate, **H**. The reported products of the alkylation of diazotates with Meerwein's reagent or alkyl iodides are azoxyalkanes, **I** in eq 3, which correspond to N-alkylation.[38]

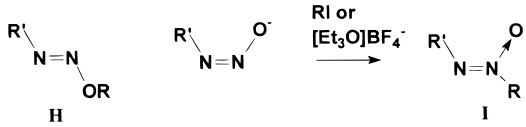

(1)

The observed and calculated vibrational data for the ONNO frameworks in **1D**, **1D**·$^1/_2$HONNOH, **2D**, and **3D** are also in fair agreement and correlate with strong coupling of the framework modes. In particular, the strongest IR active band, 1071−1061 cm^{-1}, for the products with a **D** conformation, Table 4, corresponds to an asymmetric ν(NOR) mode as the primary component, calculated to be at 1037.1 cm^{-1} in the gas phase for (*Z*)-MeON═N(O)Me, Table S9. A second strong IR active mode for these compounds is between 1487 and 1481 cm^{-1} which best correlates with the value calculated for ν_{24} at 1577.3 cm^{-1}, a mode with primarily ν(N═N) character.

In contrast with the observed structural, spectroscopic, and theoretical data for the diazenium diolates are the related data for the hyponitrite framework, such as that found in the structure of **5A**, Table 2 and Figure 3. In **5A** the observed N−N bond distance of 1.230 (3) Å is close to the typical N−N double bond even though the N(1)−O(1) distance of 1.361 (2) Å is significantly smaller than that of a typical N−O single bond. In this respect the trend observed in **5A** differs from that for *trans*-di-*O*-*tert*-butyl-hyponitrite.[17] Generally, the observed N−N double bond and N−O single bond distances are much smaller than the corresponding bond distances observed for *trans*-di-*O*-*tert*-butyl-hyponitrite,[17] by 0.022 and 0.019 Å, respectively.

(38) Moss, R. A.; Landon, M. J.; Luchter, K. M.; Mamantov, A. *J. Am. Chem. Soc.* **1972**, *94*, 4392−4394.

These structural characteristics for **5A** are consistent with the considerably higher $\nu(N-O)_{asym}$ stretching vibrational mode 1081 cm^{-1} in contrast to 1019 cm^{-1} reported for *trans*-di-*O*-*tert*-butyl-hyponitrite[17] but both are lower than the value 1093.9 cm^{-1} calculated for *trans*-dimethylhyponitrite, Table S9. In contrast with these somewhat variable results the Raman active $\nu(NN)_{sym}$ band for **5A** is at 1611 cm^{-1}, and is calculated to be at 1614.9 cm^{-1} in dimethylhyponitrite, Table S9.

Interestingly, de Sousa[39] has observed a decrease in the rate of decomposition with methyl substituents and an increase in the rate of decomposition with halide substituents in the phenyl ring relative to unsubstituted dibenzyl hyponitrite. On the basis of these observations, Sousa et al. have proposed that electron-releasing substituents increase the N−O bond order and electron-withdrawing substituents decrease the N−O bond order. The observed N−O double bond character in **5A** is in good agreement with what has been predicted by de Sousa.[39] Also supporting this conclusion is the higher thermal stability of compound **5A** (dec 86 °C) relative to the unsubstituted dibenzyl hyponitrite (dec 48 °C).[13]

p-tert-Butylbenzaldehyde is a side product, ≤14% yield, of the reaction of silver hyponitrite with *p-tert*-butylbenzyl bromide. The formation of the aldehyde most likely results from the partial decomposition and oxidation of the intermediate *trans-O-p-tert*-butylbenzyl hyponitrite, during the reaction.

Conclusions

Alkylation reactions of silver hyponitrite with *tert*-butyl bromide and *tert*-amyl bromide yield both, O/O- and N/O-dialkylated products, clearly demonstrating the ambidentate nucleophilic behavior of the hyponitrite dianion. The intermediacy of mono-O- and mono-N-alkyl species in the alkylation reactions is well established by the isolation of the two species in the protonated forms, namely, *trans*-mono-*O*-alkyl hyponitrous acid and (*Z*)-*N*-alkyl-*N*′-alkoxydiazene-*N*-oxide. Theoretical calculations suggest the presence of negative charge localization over both the oxygen and nitrogen atoms of the hyponitrite dianion, with more charge being localized over the oxygen atom. Thus, the mono-O-alkyl intermediate is clearly preferred over the N-alkyl intermediate. The isolation of the *trans*-di-O-alkyl product as the major product in each of the alkylation reactions is consistent with the theoretical results.

A comparison of the available structures of *trans*-di-*O*-alkyl hyponitrites with the structure of *trans*-di-*O-p-tert*-butylbenzyl hyponitrite reveals partial double bond character for the two N−O bonds in the latter molecule. The lower thermal stability of *trans*-di-*O-p-tert*-butylbenzyl hyponitrite in comparison to those of the analogous *tert*-butyl and *tert*-amyl derivatives is attributed to the presence of α-methylene protons and higher N−O bond order in the former compound.

Acknowledgment. We gratefully acknowledge support from the NIH (GM-53828), and the Air Force Office of Scientific Research. (Grants F49620-96-1-0417 and 98-1-0461).

Supporting Information Available: Tables S1−S8 of positional parameters, bond distances and angles, anisotropic displacement parameters, and hydrogen atom coordinates, for complexes **1D·$^1/_2$(HONNOH)** and **5A**, Table S9, listing the calculated vibrational modes for compounds discussed in the theoretical section, and Table S10, a table with complete spectroscopic data for new compounds (PDF). This material is available free of charge via the Internet at http://pubs.acs.org.

JA994261O

(39) de Sousa, J. B. *Nature* **1963**, *199*, 64−65.